Article

Phase I trial of ^{99m}Tc-1-Thio-D-glucose for imaging of lymphomas

Vladimir Chernov[1,2], Ekaterina Dudnikova[3], Roman Zelchan[1,2], Anna Medvedeva[1], Anstasiya Rybina[1], Olga Bragina[1,2], Viktor Goldberg[3], Albina Muravleva[3], Jens Sörensen[4], Vladimir Tolmachev [2,5*]

[1] Department of Nuclear Medicine, Cancer Research Institute, Tomsk National Research Medical Center, Russian Academy of Sciences, 634050 Tomsk, Russia; chernov@tnimc.ru (V.C.); zelchanrv@onco.tnimc.ru (R.Z.); medvedeva@tnimc.ru (A.M.); pankovaan@mail.ru (A.R.); rungis@mail.ru (O.B.)
[2] Research Centrum for Oncotheranostics, Research School of Chemistry and Applied Biomedical Sciences, Tomsk Polytechnic University, 634050 Tomsk, Russia;
[3] Department of Cancer Chemotherapy, Cancer Research Institute, Tomsk National Research Medical Center Russian Academy of Sciences, 634050 Tomsk, Russia; ekaterina.dudnikova@list.ru (E.D); goldbergve@mail.ru (V.G.); albina_danilova7487@mail.ru (A.M.)
[4] Radiology and Nuclear Medicine, Department of Surgical Sciences, Uppsala University, 751 83 Uppsala, Sweden; jens.sorensen@pet.uu.se
[5] Department of Immunology, Genetics and Pathology, Uppsala University, 751 83 Uppsala, Sweden vladimir.tolmachev@igp.uu.se
* Correspondence: vladimir.tolmachev@igp.uu.se; Tel.: +46 704 250782

Abstract: Like ^{18}F-FDG, ^{99m}Tc-1-thio-D-glucose (^{99m}Tc-TG) also binds to GLUT receptors. The aim of this Phase I study was to evaluate the safety, biodistribution and dosimetry of ^{99m}Tc-TG. Twelve lymphoma patients were injected with 729±102 MBq ^{99m}Tc-TG. Whole-body planar imaging was performed in 10 patients at 2, 4, 6 and 24 h after injection. In all 12 patients SPECT/CT (at 2 h) and SPECT (at 4 and 6 h) imaging was performed. Vital signs and possible side effects were monitored during imaging and up to 7 days after injection. ^{99m}Tc-TG injections were well tolerated and no side effects or alterations in blood and urine analyses data were observed. The highest absorbed dose was in the kidneys and urinary bladder wall, followed by the adrenals, prostate, bone marrow, lungs, myocardium, ovaries, uterus, liver and gall bladder wall. ^{99m}Tc-TG SPECT/CT revealed foci of high activity uptake in the lymph nodes of all nine patients with known nodal lesions. Extranodal lesions were detected in all nine cases. In one patient, a lesion in the humerus head, which was not detected by CT, was visualized using ^{99m}Tc-TG. Potentially, ^{99m}Tc-TG SPECT can be considered as an additional diagnostic method for imaging GLUT receptors in lymphoma patients.

Keywords: ^{99m}Tc-1-Thio-D-glucose, single-photon emission computed tomography, Lymphoma, Hodgkin's lymphoma, non-Hodgkin's lymphomas

1. Introduction

Positron emission tomography (PET), and more recently PET/CT, using ^{18}F-fluorodeoxyglucose (FDG) is the most sensitive and specific imaging technique currently available for patients with lymphoma. Numerous studies indicate the utility of ^{18}F-FDG PET/CT for staging lymphomas, predicting their response to therapy and evaluating their treatment effectiveness [1, 2]. Despite the advantages of this technology for patients' management, the use of PET in many developing countries is limited by the high cost of studies and low number of PET/CT facilities. However, SPECT scanners are installed in many hospitals around the world and therefore the use of tracers labeled with gamma-emitting nuclides for the imaging of hypermetabolic lesions might be a solution for these countries. Several glucose analogues have been preclinically evaluated for the SPECT imaging of tumor metabolism [3-7], of which ^{99m}Tc-1-thio-D-glucose (^{99m}Tc-TG) is one of such tracers

(Figure S1). The mechanism of how ^{99m}Tc-TG binds to malignant cells was elucidated using colorectal carcinoma (HCT-116) and human lung adenocarcinoma (A549) cells [4]. The ^{99m}Tc-TG and ^{18}F-FDG accumulation level in HCT-116 cells was very similar, while the ^{18}F-FDG uptake in the A549 cell line was almost double that of ^{99m}Tc-TG. The cellular accumulation of both ^{99m}Tc-TG and ^{18}F-FDG decreased when the glucose competitor concentration increased, but was enhanced in the presence of insulin. These facts suggested that both ^{18}F-FDG and ^{99m}Tc-TG bound to cells with the participation of glucose transport proteins. Furthermore, cellular uptake of both ^{18}F-FDG and ^{99m}Tc-TG was reduced in the presence of cytochalasin B, which blocks the GLUT1-5 channels. On the contrary, no reduction of cellular uptake was observed for either ^{99m}Tc-TG or ^{18}F-FDG when SGLT1-3 was blocked by phloretin, suggesting that these transporter proteins are not involved in the uptake process [4]. This lead to the conclusion that these agents are taken up by the cells mainly via GLUT transporters, which was in agreement with the data demonstrating a substantial overexpression of GLUT1 in the tested cell lines [8- 10]. It should be noted that in contrast to ^{18}F-FDG, which is almost completely localized in the cytoplasm, ^{99m}Tc-TG accumulates predominantly in cell membranes. This feature was explained by the large size of the ^{99m}Tc-TG molecule, which might hamper its transport into cells, and the tracer remains attached to membrane-bound transporter proteins [4]. Overall, this study suggested that ^{99m}Tc-TG could be used for the mapping of sites with elevated GLUT expression, including malignant tumors.

In preparation for clinical studies, a single-vial kit for labeling 1-thio-D-glucose and the analytical methods for characterizing the labeled product were developed [11]. Further preclinical studies demonstrated that ^{99m}Tc-TG does not have any acute or cumulative toxicity and is not allergenic. Accumulation of ^{99m}Tc-TG in tumor cells, including the RMA lymphoma cell line, was demonstrated in vivo and in vitro [11,12].

There were three primary objectives of this first-in-human study: firstly, to obtain initial information concerning the safety and tolerability of ^{99m}Tc-TG after a single intravenous injection; secondly, to assess the distribution of ^{99m}Tc-TG in normal tissues and in tumors over time; and thirdly, to evaluate the dosimetry of ^{99m}Tc-TG.

The secondary objective was to evaluate the possibility of using ^{99m}Tc-TG SPECT/CT for visualizing GLUT expression in the nodal and extranodal lesions of lymphoma patients.

2. Materials and Methods

2.1. Patients

This was a prospective, open-label, non-randomized diagnostic study in patients with untreated lymphoma (ClinicalTrials.gov Identifier: NCT04292626). The protocol was approved by the Scientific Council of Cancer Research Institute and Board of Medical Ethics, Tomsk National Research Medical Center of the Russian Academy of Sciences. All subjects signed written informed consent forms.

Patients (18-70 years) with lymphoma were eligible and accepted based on the following inclusion criteria: (1) clinical and radiological diagnosis of Hodgkin lymphoma and non-Hodgkin lymphoma with immunohistologic verification; (2) volumetrically quantifiable tumor lesions on CT or ultrasound, with at least one lesion > 1.0 cm in greatest diameter; (3) hematological, liver and renal function test results within the normal limits; (4) negative pregnancy test for female patients of childbearing potential; and (5) capability to undergo the diagnostic investigations planned in the study.

Patients (18-70 years) with lymphoma were not accepted based one or more of the following exclusion criteria: (1) a previous diagnosis with an autoimmune disease; (2) an active infection or history of severe infection; (3) known to be HIV positive or have a

Preprints (www.preprints.org) | NOT PEER-REVIEWED | Posted: 5 May 2022 doi:10.20944/preprints202205.0028.v1

chronically active hepatitis B or C infection; or (4) had been administered other investigational medicinal products.

Twelve patients (four male and eight female) were enrolled (Table 1, Figure S2) and, as a local standard of care, chest and abdomen CT (Siemens Somatom Emotions 16 ECO) and ultrasound (GE LOGIQ E9) imaging was performed along with biopsy sampling for all patients. Biopsy samples of nodal and extranodal lesions were collected and the diagnosis was verified by immunohistochemistry (IHC).

Table 1. Patient characteristics before injection with ^{99m}Tc-TG.

Patient no	Sex	Age (y)	IHC diagnosis	Stage
1	Male	62	FL	IVA
2	Male	39	HL	IVA
3	Female	20	HL	IIIB
4	Female	57	DLBCL	IVB
5	Female	49	MALT-lymphoma	IIIB
6	Female	56	BLL	IVA
7	Male	58	FL	IVA
8	Female	45	HL	IIA
9	Male	68	DLBCL	IVA
10	Female	39	MZL	IVA
11	Female	34	HL	IIIB*
12	Female	61	DLBCL	IVA

FL - Follicular lymphoma; HL - Hodgkin lymphoma; DLBCL - Diffuse large B-cell lymphoma; MALT-lymphoma - mucosa-associated lymphoid tissue lymphoma; BLL - B-lymphoblastic lymphoma; MZL – Marginal zone lymphoma. * - stage was changed to IVB based on ^{99m}Tc-TG SPECT/CT and additional MRI studies performed after ^{99m}Tc-TG SPECT/CT.

2.2. Imaging protocol

Labeling of ^{99m}Tc-TG was performed in aseptic conditions using a single-vial kit described earlier [11]. The radiochemical purity of ^{99m}Tc-TG was 97±1 %.

The ^{99m}Tc-TG, in a dose of 729±102 MBq, was injected as an intravenous bolus. Imaging was performed using a Siemens Symbia Intevo Bold scanner equipped with a high-resolution low-energy collimator. Anterior and posterior whole-body planar imaging (at a scan speed of 12 cm/min, 1024x256 pixel matrix) was carried out in patients 1-10 at 2, 4, 6 and 24 h after injection. All 12 patients received SPECT/CT scans (SPECT:60 projections, 20 seconds each, 256x256 pixel matrix; CT: 130 kV, effective 36 mAs) at 2 h and only SPECT scans (60 projections, 20 seconds each, 256x256 pixel matrix) 4 and 6 h after injection.

2.3. Evaluation of distribution and dosimetry

Regions of interest (ROI) were drawn over organs of interest and the body contour on the anterior and posterior whole-body images. A geometric mean of counts at 2, 4, 6 and 24 h was calculated for each ROI. For quantification, a known activity of ^{99m}Tc in a water-filled phantom in combination with Chang's correction was used. A ROI was placed over the heart to assess the activity in the blood. Data were fitted to single exponential functions and residence times were calculated as areas under fitted curves using Prism 8 (GraphPad Software, LLC). Absorbed doses were calculated by OLINDA/EXM 1.1 using an adult female and male phantom.

To calculate tumor-to-background ratios at 2, 4 and 6 h, a one cm^3 volume of interest (VOI) was drawn on tomograms centered on the highest tumor uptake, and counts were recorded. Thereafter, this VOI was copied to the contralateral side to obtain reference counts. The maximal standard uptake value (SUVmax) in nodal or extranodal lesions with the highest ^{99m}Tc-TG accumulation was calculated 2 h after injection, when CT data was available. Tumor sizes were defined by CT as the maximum size of the largest lesion.

2.4. Statistics

Values are reported as mean ± standard deviation. The significance of differences between uptakes in organs at different time points was analyzed using 1-way ANOVA.

3. Results

3.1. Safety and tolerability

The intravenous bolus administration of ^{99m}Tc-TG was well tolerated by all 12 patients. No changes in vital signs or adverse reactions were registered during imaging or the follow-up period. No relevant changes in blood or urine samples were found after their analyses.

3.2. Evaluation of distribution and dosimetry

The kinetics of ^{99m}Tc-TG elimination from blood is shown in Figure S3. The elimination half-lives were 3.1 h (95% CI 1.3 to 16 h) in female patients and 3.6 h (95% CI 1.6 to 19 h) in male patients.

The kidneys, liver and lungs were the organs with the highest accumulation of activity (Table 2; Fig. 1). Noticeable activity was also observed in the gall bladder, spleen, thyroid, small intestines, testes and stomach. No significant difference between male and female patients was found.

Table 2. Decay-corrected uptake of ^{99m}Tc in the highest-uptake organs based on planar imaging of tumor-free areas. The data are presented as average %ID ± SD per organ for six females and four males at different time points after injection with ^{99m}Tc-TG.

	Kidney		Liver		Lung	
Time	Female	Male	Female	Male	Female	Male
2 h	5.6±2.7	4.0±0.7	3.5±1.1	3.4±1.0	4.0±1.5	4.6±1.1
4 h	6.5±3.5	4.3±0.9	3.6±0.8	3.2±0.8	4.5±2.1	4.0±0.9
6 h	5.9±3.1	3.7±1.3	3.9±1.2	2.5±0.8	3.7±1.2	3.1±1.1
24 h	7.1±3.7	4.5±2.1	2.9±1.1	2.6±0.5	2.7±1.0	2.5±0.5

The evaluation of the absorbed doses is shown in Table 3. The highest absorbed dose was in the kidneys and urinary bladder wall, followed by the adrenals, prostate, osteogenic cells, lungs, heart wall, ovaries, uterus, liver and gall bladder wall. The effective doses were 0.0072±0.0036 and 0.0135±0.0091 mSv/MBq for female and male patients, respectively. For a typical injected activity of 730 MBq, which was used in this study, an expected effective dose would be 5.0-9.8 mSv.

3.3. ^{99m}Tc-TG SPECT/CT imaging of nodal and extranodal lesions

According to standard diagnostic methods (clinical examination, CT and ultrasound), lymph node lesions were known in 9 of the 12 examined lymphoma cases and extranodal lesions also in 9 of the patients. The ^{99m}Tc-TG SPECT/CT scans revealed foci of elevated radiopharmaceutical uptake in the lymph nodes of all nine patients with nodal lesions (example in Fig. 2). Extranodal lesions were also detected by ^{99m}Tc-TG SPECT in all nine of the known cases. ^{99m}Tc-TG SPECT/CT correctly visualized brain (Fig. 3), neck, chest (Fig. 4), and abdominal lesions (Fig. 5). In one patient, according to ^{99m}Tc-TG SPECT/CT, a lesion in the humerus head was visualized, which was not detected by CT (Fig. 6A). Based on this finding, MRI of the left shoulder joint was performed and a lymphoma lesion in the metaepiphysis of the humerus was confirmed (Fig. 6B) and the stage of the disease was changed from IIIB to IVB. In the highest ^{99m}Tc-TG accumulating lesions, SUVmax was 2.6±1.1 at 2 h after injection (Table 4). The tumor/contralateral background ratios reached 4.8±5.4 at 2 hours after injection, decreased to 3.6±4.8 after 4 hours and did not change significantly after that (Table 4).

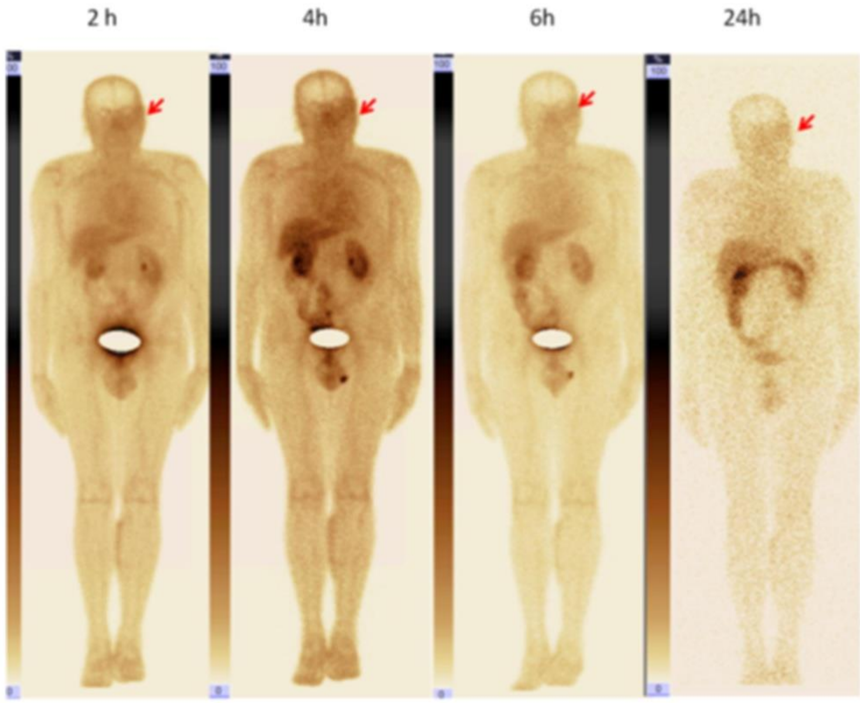

Figure 1. Anterior images of patient 7 (male) at 2, 4, 6, and 24 h after injection of ^{99m}Tc-TG. Activity in the urinary bladder is masked. The upper setting of the scale window is 100 % of the maximum counts.

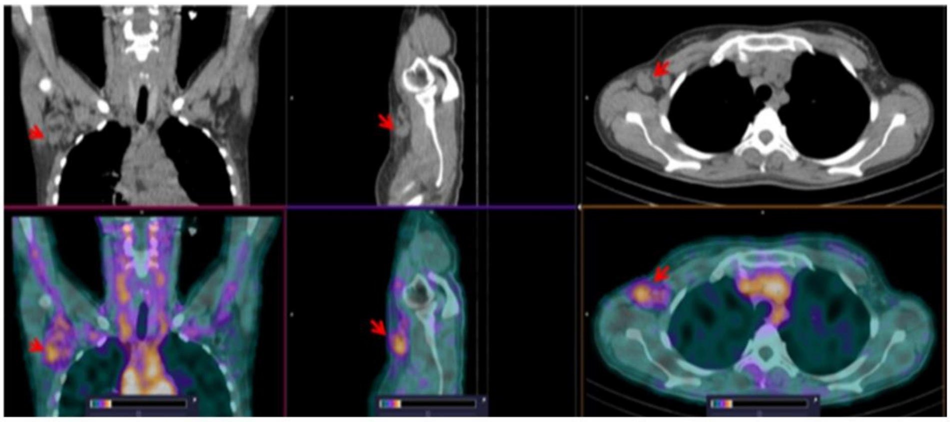

Figure 2. SPECT/CT images of patient 11 at 2 h after injection of ^{99m}Tc-TG. An enlarged (up to 2.2 cm) right axillary node with elevated ^{99m}Tc-TG uptake (SUVmax=1.86) is visualized (arrows). The upper setting of the scale window (22% of the maximum number) was adjusted to visualize the lesion.

doi:10.20944/preprints202205.0028.v1

Table 3. Absorbed doses (mGy/MBq) after injection of ^{99m}Tc-TG.

Site	Female patients	Male patients
Testes		0.013±0.011
Brain	0.0017±0.0006	0.0012±0.0003
Breasts	0.0018±0.0011	0.0011±0.0002
Skin	0.0019±0.0007	0.0014±0.0003
Muscle	0.0026±0.0011	0.0021±0.0005
Red Marrow	0.0034±0.0013	0.0026±0.0005
Stomach Wall	0.0042±0.0014	0.0028±0.0005
Small Intestine	0.0049±0.0020	0.0042±0.0009
LLI Wall	0.005±0.003	0.005±0.003
Thymus	0.005±0.002	0.005±0.001
Thyroid	0.005±0.002	0.004±0.001
Spleen	0.0051±0.0019	0.0032±0.0006
Pancreas	0.0052±0.0016	0.0033±0.0004
ULI Wall	0.0053±0.0020	0.0038±0.0008
Gallbladder Wall	0.007±0.003	0.005±0.001
Liver	0.007±0.002	0.004±0.001
Uterus	0.007±0.004	
Ovaries	0.0074±0.0035	
Heart Wall	0.008±0.003	0.006±0.002
Lungs	0.008±0.003	0.005±0.001
Osteogenic Cells	0.008±0.003	0.006±0.001
Adrenals	0.009±0.003	0.005 ±0.001
Kidneys	0.03±0.01	0.02±0.00
Urinary Bladder Wall	0.03±0.04	0.05±0.05
Prostate		0.010±0.006
Total Body	0.0038±0.0015	0.0028±0.0005
Effective Dose Equivalent (mSv/MBq)	0.0093±0.0047	0.0171±0.0114
Effective Dose (mSv/MBq)	0.0072±0.0036	0.0135±0.0091

Preprints (www.preprints.org) | NOT PEER-REVIEWED | Posted: 5 May 2022 doi:10.20944/preprints202205.0028.v1

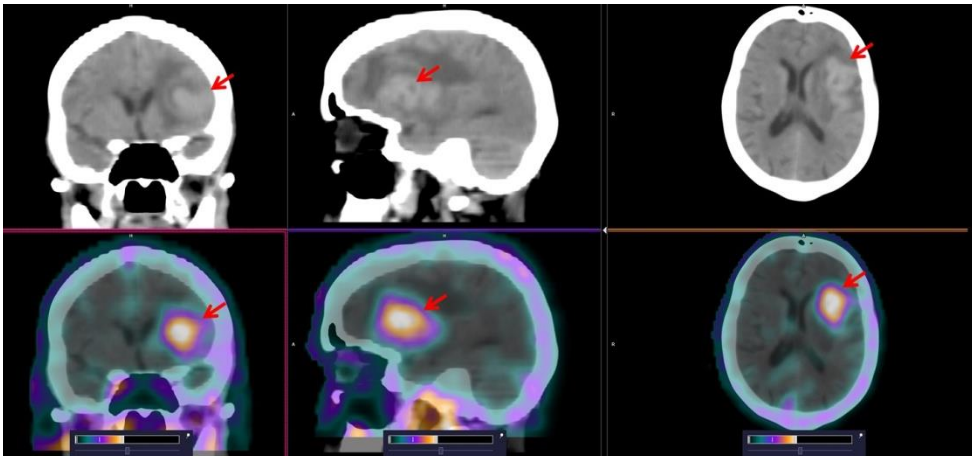

Figure 3. SPECT/CT images of patient 12 at 2 h after injection of ^{99m}Tc-TG. High ^{99m}Tc-TG uptake in left frontoparietal region of the brain (SUVmax=2.65) is visualized (arrows). The upper setting of the scale window (65% of the maximum number) was adjusted to visualize the lesion.

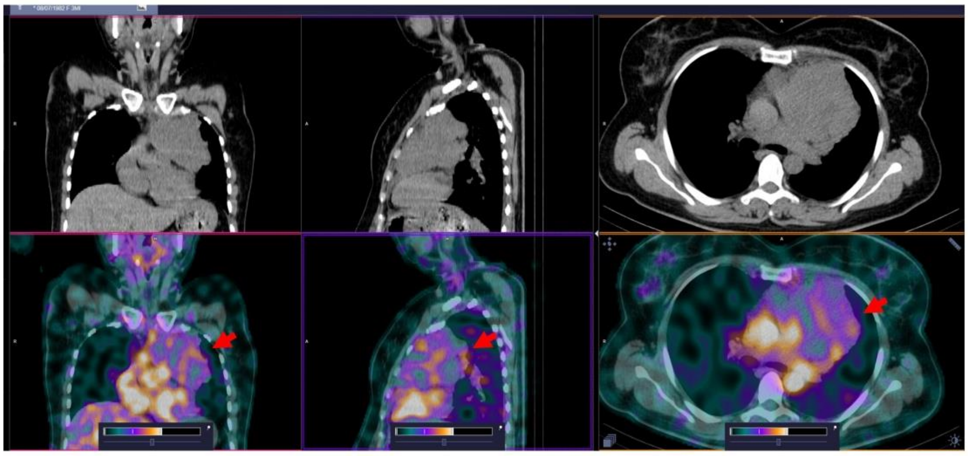

Figure 4. SPECT/CT images of patient 3 at 2 h after injection of ^{99m}Tc-TG. Elevated ^{99m}Tc-TG uptake in the mediastinal tumor (SUVmax=1.3) is visualized (arrows). The upper setting of the scale window (60% of the maximum number) was adjusted to visualize the lesion.

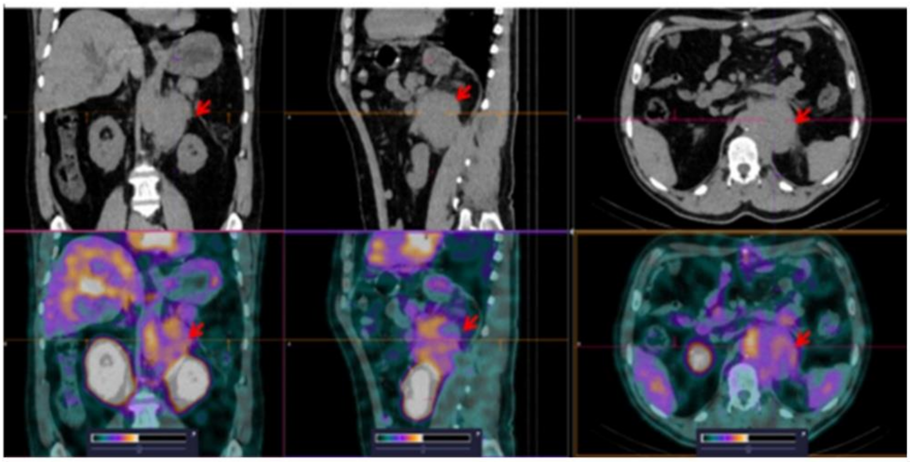

Figure 5. SPECT/CT images of patient 1 at 2 h after injection of ^{99m}Tc-TG. Elevated ^{99m}Tc-TG uptake in the retroperitoneal tumor (SUVmax=3.92) is visualized (arrows). The upper setting of the scale window (40% of the maximum number) was adjusted to visualize the lesion.

Table 4. Tumor size, SUVmax (at 2 h) and tumor-to-contralateral site ratios (at 2, 4 and 6 h) after the injections of ^{99m}Tc-TG.

Patients	Tumor size cm	SUV max tumor	SUV max gallbladder	Tumor/ background 2 h	Tumor/ background 4 h	Tumor/ background 6 h
1.	8.0	3.92	4.2	4.1	4.2	2.7
2.	1.8	2.23	7.1	2.5	1.6	1.4
3.	12.0	1.3	-	2.5	1.6	1.8
4.	3.8	4.53	2.9	1.7	1.9	1.9
5.	3.6	3.39	20.9	3.5	1.4	1.3
6.	4.6	3.34	4.2	3.6	1.6	1.7
7.	5.0	2.45	-	2.5	1.7	1.6
8.	4.5	1.43	-	3.8	2.5	2.8
9.	2.8	1.89	-	2.8	1.3	1.48
10.	8.3	1.21	-	2.9	1.7	3.2
11.	4.2	2.28	3.5	6.3	5.8	4.2
12.	4.6	2.65	-	21.9	18.3	16.1
Mean± SD	5.3±2.8	2.6±1.1	4.4±1.60*	3.3±1.2**	2.30±1.42** P=0.005***	2.19±0.91** P=0.005***

* - Mean±SD was calculated for normal ^{99m}Tc-TG gallbladder uptake, ** values for extracranial lesions; *** the significance of the differences is shown in comparison with the tumor/background value for extracranial lesions at 2 hours.

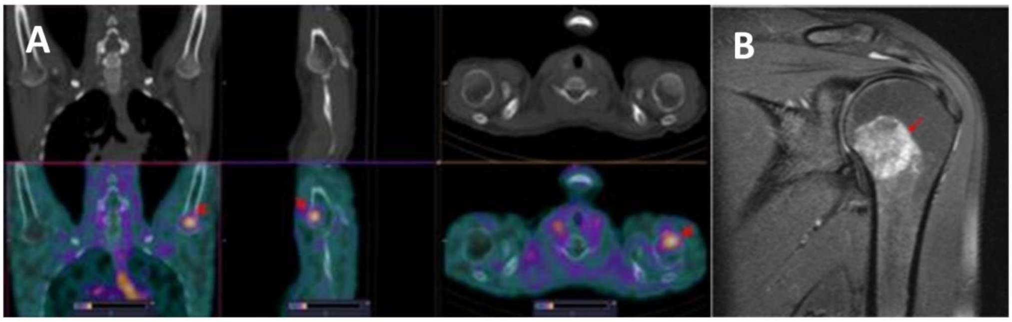

Figure 6. A) SPECT/CT images of patient 11 at 2 h after injection of ^{99m}Tc-TG. Elevated ^{99m}Tc-TG uptake in the humerus head (SUVmax=2.28) is visualized (arrows). No pathological changes were found using CT. The upper setting of the scale window (22% of the maximum number) was adjusted to visualize the lesion. B) MRI image of the left shoulder joint, T1

In our study, patient 5 had cholecystitis as a concomitant diagnosis. In this case, a high ^{99m}Tc-TG uptake (SUVmax=20.89 vs 4.38±1.60 in normal patients) in the gallbladder was found (Figure 7, Table 4). In the rest of the patients, elevated ^{99m}Tc-TG accumulation in the gallbladder was not visualized (Figure 7, Table 4).

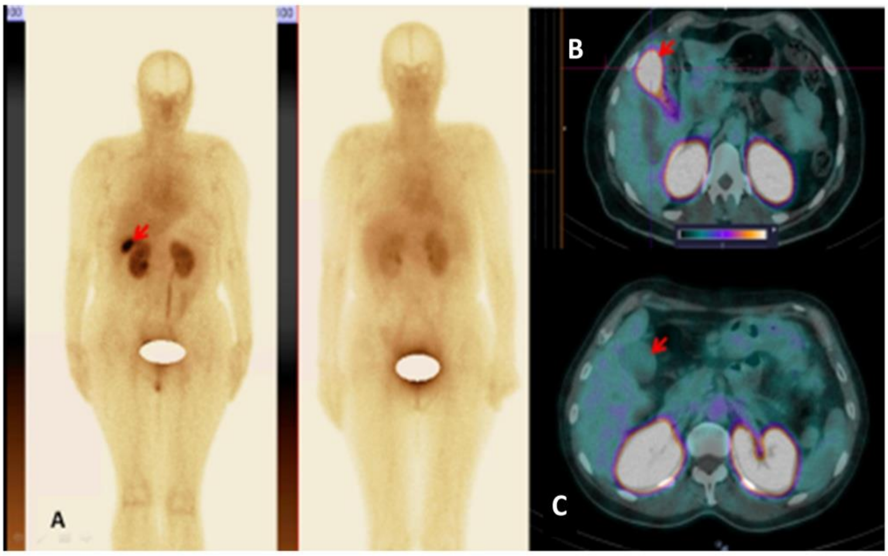

Figure 7. A) Anterior images of female patient 5 (left) and female patient 4 (right) at 2 h after injection of ^{99m}Tc-TG. High ^{99m}Tc-TG uptake in the gallbladder in patient 5 is visualized (arrow). The upper setting of the scale window is 100 % of the maximum counts. B) SPECT/CT image of patient 5 at 2 h after injection of ^{99m}Tc-TG. High ^{99m}Tc-TG uptake (SUVmax=20.89) in the gallbladder in Patient 5 is visualized (arrow). C) SPECT/CT image of patient 4 at 2 h after injection. There is no pathological uptake in the gallbladder of patient 4 (SUVmax=2.87) (arrow). The upper setting of the scale window (100% of the maximum number).

4. Discussion

This study demonstrated that the injection of ^{99m}Tc-TG is well-tolerated and not associated with any adverse effects. The favorable dosimetry properties of ^{99m}Tc ensured a moderate effective dose. In the current study, typical equivalent doses were 5.0-9.8 mSv. However, the injected activity in this study was specifically selected to obtain good counting statistics 24 h after injection for dosimetry calculations. For routine use, the injected activity could be reduced at least 3-fold (see below) with a proportional reduction in the effective dose. For comparison, a typical effective dose from ^{18}F-FDG PET is 3.5 mSv when 185 MBq is administered [13].

^{99m}Tc-TG SPECT allowed us to identify foci corresponding to all nodal lesions found according to the standard diagnostic methods in this study. There was also an excellent correlation between visualizing extranodal lesions using ^{99m}Tc-TG SPECT and the standard diagnostic methods in all cases of brain (Fig. 3), neck, chest (Fig. 4), and abdominal lesions (Fig. 5). A major advantage of ^{18}F-FDG PET/CT over CT is the possibility to detect bone marrow lesions in lymphomas, since CT allows visualization only in the case of bone destruction [14]. The use of ^{99m}Tc-TG SPECT enabled detection of a bone lesion, which was not visualized by CT (Fig. 6A). This finding prompted an additional MRI examination which confirmed a lymphoma lesion in the humerus (Fig. 6B). For this patient, the stage of the disease was changed based on ^{99m}Tc-TG SPECT imaging followed by MRI confirmation.

Because the tumor-to-background ratio reached 3.3±1.2 at 2 hours after injection, then decreased to 2.30±1.42 after 4 hours and after that did not change significantly, the optimal time for SPECT imaging is 2 hours after the injection. At this time point, the ^{99m}Tc-TG SUVmax was 2.6±1.1, which is considerably lower than the typical ^{18}F-FDG SUVmax in lymphoma lesions according to the literature [15]. A possible explanation for this is that ^{99m}Tc-TG is not internalized after binding to GLUT1 to the same extent as ^{18}F-FDG [4] and does not undergo metabolic trapping. Since ^{99m}Tc-TG is likely imaging GLUT-receptor expression rather than glucose metabolism, it will be essential for future clinical applications to confirm that the uptake of ^{99m}Tc-TG in the rest of the human body is also GLUT-mediated. It is well known that GLUT receptors are overexpressed in inflammatory cells leading to an active uptake of ^{18}F-FDG in inflammatory foci [16]. In particular, an accumulation of ^{18}F-FDG in cholecystitis has been previously demonstrated [17-19]. For the study herein, imaging of patient 4 with documented chronic cholecystitis showed a much higher activity accumulation in the gallbladder, compared to other patients (Table 4; Fig. 7). This suggests that ^{99m}Tc-TG uptake is dependent on GLUT-receptor expression, similarly to ^{18}F-FDG, which might support its use for the imaging of hypermetabolic lesions overexpressing these receptors. Unfortunately, this also means that all pitfalls and artifacts known when using ^{18}F-FDG for the imaging of hematologic malignancies [20] might also apply when using ^{99m}Tc-TG.

Currently, ^{18}F-FDG PET is applied for post-therapy-response assessment in "FDG-avid" lymphomas [21, 22]. Investigating the use of ^{99m}Tc-TG for this application might also be worthwhile, taking into account that current SPECT/CT technology permits the semi-quantitative assessment of uptake.

Another interesting finding is that ^{99m}Tc-TG is not accumulated in the brain, despite GLUT1 being the main transporter for glucose through the intact blood-brain barrier [23]. This might be because the transport of ^{99m}Tc-TG through cellular membranes is impaired [4]. This phenomenon might facilitate the use of ^{99m}Tc-TG for the visualization of lymphoma-associated brain lesions (Fig. 3) and brain tumors, where the blood-brain-barrier is typically disrupted.

Obviously, ^{99m}Tc-TG SPECT/CT cannot compete with ^{18}F-FDG PET/CT in countries where PET is available. First, the accumulation of ^{18}F-FDG in lymphoma lesions is higher, which is a prerequisite for better imaging contrast. Second, sensitivity and quantification accuracy of PET is better. Still, ^{99m}Tc-TG might be the only tracer for molecular imaging of lymphoma for patients living in countries with poor or no access to PET. Therefore, we believe that further clinical development of this tracer is warranted.

5. Conclusions

Injections of ^{99m}Tc-TG appear safe and the radiation burden was comparable to the burden from ^{18}F-FDG. The ^{99m}Tc-TG showed an elevated uptake in the nodal and extranodal lesions in malignant lymphomas patients. Further studies concerning the use of ^{99m}Tc-TG SPECT/CT for lymphoma staging and therapy monitoring are justified.

Supplementary Materials: The following are available online **Figure** S1**.** Structure of ^{99m}Tc-1-thio-D-glucose; **Figure** S2. Standards for Reporting of Diagnostic Accuracy Studies (STARD) flow diagram; Figure S3. Kinetics of elimination of ^{99m}Tc-TG from blood. Data are based on count rates in regions of interest placed over hearts. %ID = percentage injected dose.

Author Contributions: Conceptualization, V.C., V.T. and J.S.; methodology, V.C., V.T., E.D., V.G. and J.S.; formal analysis, V.C., E.D. and V.T.; investigation, R.Z, A.M., O.B., A.R.; E.D., A.M. and V.G.; resources, V.C., V.T. and V.G.; data curation, V.C. and V.T.; writing—original draft preparation, V.C.; writing—review and editing, V.T. R.Z,, A.M., O.B., A.R.; E.D., A.M. and V.G.;and J.S.; visualization, R.Z, A.M., O.B. and A.R.; supervision, V.C., V.T. and V.G.; project administration, V.C., V.T. and V.G.; funding acquisition, V.T. All authors have read and agreed to the published version of the manuscript.

Funding: This research was funded by the Ministry of Science and Higher Education of the Russian Federation (075-15-2019-1925).

Institutional Review Board Statement: Clinical studies were planned in agreement with Federal Law "On Provision of Medicines" dated April 12, 2010 № 61-FZ and were approved by the Scientific Council of Cancer Research Institute and Board of Medical Ethics, Tomsk National Research Medical Center of the Russian Academy of Sciences. (ethical permission 7).

Informed Consent Statement: Informed consent was obtained from all subjects involved in the study.

 doi:10.20944/preprints202205.0028.v1

Data Availability Statement: Data is contained within the article. .

Conflicts of Interest: No conflicts of interest

References

1. Barrington SF, Mikhaeel NG, Kostakoglu L, Meignan M, Hutchings M, Müeller SP et al. Role of imaging in the staging and response assessment of lymphoma: consensus of the International Conference on Malignant Lymphomas Imaging Working Group. *J Clin Oncol*. 2014;32:3048-3058.
2. Cheson BD, Fisher RI, Barrington SF, Cavalli F, Schwartz LH, Zucca E et al. , Recommendations for initial evaluation, staging, and response assessment of Hodgkin and non-Hodgkin lymphoma: the Lugano classification. J Clin Oncol. 2014;32:3059-68.
3. Jun Oh S, Ryu JS, Yoon EJ, Bae MS, Choi SJ, Park KB, Moon DH. ^{99m}Tc-labeled 1-thio-beta-D-glucose as a new tumor-seeking agent: synthesis and tumor cell uptake assay. *Appl Radiat Isot*. 2006;64:207-215.
4. Seidensticker M, Ulrich G, Muehlberg FL et al. Tumor cell uptake of ^{99m}Tc-labeled 1-thio-β-D-glucose and 5-Thio-D-glucose in comparison with 2-Deoxy-2-[^{18}F]fluoro-D-glucose in vitro: kinetics, dependencies, blockage and cell compartment of accumulation. *Mol Imaging Biol*. 2014;16:189-198.
5. Dapueto R, Aguiar RB, Moreno M, Machado CM, Marques FL, Gambini JP, Chammas R, Cabral P, Porcal W. Technetium glucose complexes as potential cancer imaging agents. *Bioorg Med Chem Lett*. 2015;25:4254-4259.
6. Zhang X, Ruan Q, Duan X et al. Novel 99mTc-labeled glucose derivative for single photon emission computed tomography: a promising tumor imaging agent. *Mol Pharm*. 2018;15:3417-3424.
7. Gan Q, Zhang X, Ruan Q, Fang S, Zhang J. 99mTc-CN7DG: A highly expected SPECT imaging agent of cancer with satisfactory tumor uptake and tumor-to-nontarget ratios. *Mol Pharm*. 2021;18:1356-1363.
8. Ong LC, Jin Y, Song IC et al. 2-[^{18}F]-2-deoxy-D-glucose (FDG) uptake in human tumor cells is related to the expression of GLUT-1 and hexokinase II. *Acta Radiol*. 2008;49:1145–1153.
9. Guo GF, Cai YC, Zhang B. et al. Overexpression of SGLT1 and EGFR in colorectal cancer showing a correlation with the prognosis. *Med Oncol*. 2011;28(Suppl 1):S197–203.
10. Huber SM, Misovic M, Mayer C. et al. EGFR-mediated stimulation of sodium/glucose cotransport promotes survival of irradiated human. *Radiother Oncol*. 2012; 103:373–379.
11. Stasyuk E, Skuridin V, Rogov A et al. ^{99m}Tc-labeled monosaccharide kits: development methods and quality control. *Sci Rep*. 2020;10:5121.
12. Zeltchan R, Medvedeva A, Sinilkin I et al. Study of potential utility of new radiopharmaceuticals based on technetium-99m labeled derivative of glucose. *AIP Conference Proceedings*. 2016;1760:020072 https://doi.org/10.1063/1.4960291
13. Boellaard R, Delgado-Bolton R, Oyen WJ et al. European Association of Nuclear Medicine (EANM). FDG PET/CT: EANM procedure guidelines for tumour imaging: version 2.0. *Eur J Nucl Med Mol Imaging*. 2015;42:328-354.
14. Adams HJA, Kwee TC. Value of detecting bone marrow involvement in Hodgkin lymphoma. B*r J Haematol*. 2019;187:397-399.
15. Li H, Wang X, Zhang L, Yi X, Qiao Y, Jin Q. Correlations between maximum standardized uptake value measured via 18F-fluorodeoxyglucose positron emission tomography/computed tomography and clinical variables and biochemical indicators in adult lymphoma. *J Can Res Ther*. 2019;15:1581-1588.
16. Meller J, Sahlmann CO, Scheel AK. 18F-FDG PET and PET/CT in fever of unknown origin. *J Nucl Med*. 2007;48:35-45.
17. Yu JQ, Kung JW, Potenta S, Xiu Y, Alavi A, Zhuang H. Chronic cholecystitis detected by FDG-PET. *Clin Nucl Med*. 2004;29:496-497.
18. Kitazono MT, Colletti PM. FDG PET imaging of acute cholecystitis. *Clin Nucl Med*. 2006;31:23-24.
19. Nasseri Y, Ourian AJ, Waxman A, D'Angolo A, Thomson LE, Margulies DR. Fluorodeoxyglucose positron emission tomography-computed tomography: a novel approach for the diagnosis of cholecystitis for equivocal diagnoses after ultrasound imaging. *Am Surg*. 2012;78:1109-1113.
20. Pilkington P, Lopci E, Adam JA, Kobe C, Goffin K, Herrmann K. FDG-PET/CT Variants and Pitfalls in Haematological Malignancies. *Semin Nucl Med*. 2021;51:554-571.
21. Kobe C, Dietlein M, Hellwig D. PET/CT for Lymphoma Post-therapy Response Assessment in Hodgkin Lymphoma and Diffuse Large B-cell Lymphoma. *Semin Nucl Med*. 2018;48:28-36.
22. Karls S, Shah H, Jacene H. PET/CT for Lymphoma Post-therapy Response Assessment in Other Lymphomas, Response Assessment for Autologous Stem Cell Transplant, and Lymphoma Follow-up. *Semin Nucl Med*. 2018;48:37-49.
23. Patching SG. Glucose Transporters at the Blood-Brain Barrier: Function, Regulation and Gateways for Drug Delivery. *Mol Neurobiol*. 2017;54:1046-1077.